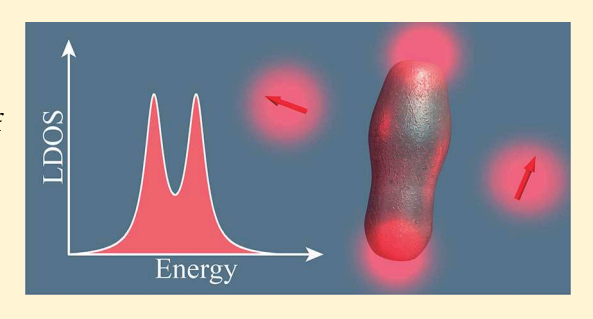
Analysis of the Limits of the Local Density of Photonic States near **Nanostructures**

Stephen Sanders and Alejandro Manjavacas*

Department of Physics and Astronomy, University of New Mexico, Albuquerque, New Mexico 87131, United States

Supporting Information

ABSTRACT: Nanostructures with sizes smaller than or comparable to visible light strongly modify the decay rate of dipole emitters placed in their vicinity. Such modification is usually characterized using the local density of photonic states (LDOS), which quantifies the availability of photonic states at a certain position and frequency in the presence of a nanostructure. Here, we present a detailed analysis of the limits of this quantity through the study of a sum rule that bounds its spectral integral, taking into account both its radiative and nonradiative components. The sum rule studied here relates the integral over the spectrum of the LDOS at a certain point to the field induced by a static dipole placed at that same location. We confirm the validity of this sum



rule and investigate its implications for the response of nanostructures by performing rigorous numerical calculations for a variety of systems, including nanospheres, nanodisks, and films, made of different metallic and dielectric materials, as well as graphene. Furthermore, we apply the sum rule to the cross density of photonic states (CDOS), a quantity that characterizes the spatial coherence of light in the presence of a nanostructure and determines, as well, the interaction between two dipole emitters located in its vicinity. We show how this result can be used as a guide to select the most favorable nanostructure geometries and materials to achieve strong values of the LDOS and the CDOS over desired parts of the spectrum, thus helping to engineer strong decay rates and coupling enhancements near nanostructures.

KEYWORDS: local density of photonic states, decay rate, sum rule, plasmons, nanoparticles

 $^{
m extsf{T}}$ he ability of metallic nanostructures to support surface $oldsymbol{oldsymbol{\bot}}$ plasmons, which interact strongly with light and concentrate it into volumes below the diffraction limit, has opened many research opportunities, with applications to solar energy harvesting,² photocatalysis,^{3,4} biosensing,^{5,6} and nanoscale light emission, 7,8 among others. In order to exploit this ability, it is necessary to design nanostructures capable of maximizing their interaction with light over the spectral range of interest. This requires, in addition to an adequate choice of material, the engineering of the nanostructure geometry to achieve the desired near- or far-field response. 10 Such efforts can benefit extraordinarily from the knowledge of the fundamental limits on the optical response of nanostructures. To this end, there has been significant research activity focused on placing bounds on different frequency-dependent quantities. These include the extinction, scattering, and absorption cross sections of individual and interacting to nanostructures, as well as two-dimensional systems. 17

Problems involving broad frequency ranges can benefit to a greater extent from limits on spectrally integrated quantities, which are usually cast in the form of sum rules. Indeed, sum rules are ubiquitous in optics; they serve to impose constraints on the refractive index of materials, 18,19 having important implications on novel applications such as negative refraction,²⁰ as well as on the mean free path of light propagating in random media.²¹ A paradigmatic example is the Thomas-Reiche-Kuhn

sum rule, 22,23 also known as f-sum rule, which was derived in the context of electronic transitions.²⁴ This sum rule relates the integral of the extinction cross section of a nanostructure to the number of electrons that it contains 25,26 and therefore establishes an upper bound to the interaction of nanostructures with far-field radiation. On the other hand, the interaction of nanostructures with near-field sources, such as quantum emitters (i.e., atoms, molecules, quantum dots, etc.), is usually characterized through the local density of photonic states (LDOS). 1,27-32 As its name indicates, the LDOS measures the number of photonic states per unit of frequency and volume at a certain position and frequency due to the presence of a nanostructure. This quantity is closely related to the strength of the near-field associated with the photonic modes supported by the nanostructure³³ and determines the decay rate of a dipole emitter placed at that position through the so-called Purcell effect. 1,34-38 Of note is that the LDOS describes both the radiative and nonradiative channels through which the emitter can decay³⁹ (i.e., into photons and heat, respectively) and, therefore, completely characterizes the optical response of the nanostructure under near-field dipole excitation.

In the past, different sum rules involving the LDOS have been presented. Barnett and Loudon derived a sum rule for the

Received: February 16, 2018 Published: March 5, 2018



radiative component of the LDOS near nonabsorbing dielectric nanostructures, 40,41 which establishes a limit to the spectrally integrated radiative decay rate of a dipole emitter placed near a nanostructure. This sum rule was later extended by Scheel to include systems with absorption. However, if the system has absorption, the emitter can also decay nonradiatively, which is reflected in a potentially significant contribution from the nonradiative component of the LDOS. This is especially relevant for emitters placed near metallic nanostructures supporting plasmonic modes. More recently, the generalization of that sum rule for the full LDOS, including the nonradiative component, has been presented in the context of Förster resonance energy transfer (FRET).

Here, we perform a comprehensive analysis of this sum rule, which includes both the radiative and nonradiative components of the LDOS. More specifically, it connects the spectral integral of the LDOS at a certain position with the field induced by a static dipole placed at that same location. Through the rigorous solution of Maxwell's equations, we show that the sum rule is satisfied by a wide variety of systems, composed of both finite and extended structures made of different materials, including dielectrics and metals, as well as graphene. Furthermore, we investigate the application of this sum rule to the cross density of photonic states (CDOS), 31,32 which quantifies the spatial coherence of light near a nanostructure and determines the interaction between two dipole emitters placed nearby. 45 Through these analyses, we show that the LDOS sum rule can be used as a guide to design nanostructures producing strong values of LDOS and CDOS in their vicinity.

■ RESULTS AND DISCUSSION

The projected LDOS along direction $\hat{\mathbf{n}}$, evaluated at a point \mathbf{r} and frequency ω , can be calculated as (note that we use Gaussian units)

$$LDOS_{\hat{\mathbf{n}}}(\mathbf{r}, \omega) = -\frac{2\omega}{\pi} Im\{\hat{\mathbf{n}} \cdot \mathbf{G}(\mathbf{r}, \mathbf{r}, \omega) \cdot \hat{\mathbf{n}}\}$$
(1)

where $G(r, r', \omega)$ is the Green tensor of Maxwell's equations, defined as the solution of 1

$$\nabla \times \nabla \times \mathbf{G}(\mathbf{r}, \mathbf{r}', \omega) - k^{2} \varepsilon(\mathbf{r}, \omega) \mathbf{G}(\mathbf{r}, \mathbf{r}', \omega)$$
$$= -\frac{1}{c^{2}} \delta(\mathbf{r} - \mathbf{r}') \mathbf{I}$$

Here, $k = \omega/c$ and $\varepsilon(\mathbf{r}, \omega)$ is the dielectric response of the system. The Green tensor $\mathbf{G}(\mathbf{r}, \mathbf{r}', \omega)$ determines the electric field produced at \mathbf{r} by a current density distribution $\mathbf{j}(\mathbf{r}', \omega)$, oscillating at frequency ω , according to

$$\mathbf{E}(\mathbf{r},\,\omega) = -4\pi i\omega \int \mathbf{G}(\mathbf{r},\,\mathbf{r}',\,\omega) \cdot \mathbf{j}(\mathbf{r}',\,\omega) \,d\mathbf{r}'$$

The projected LDOS, defined in eq 1, governs the decay rate $\Gamma_{\hat{\mathbf{n}}}(\mathbf{r},\omega)$ of a dipole emitter oscillating along the direction of $\hat{\mathbf{n}}$, through the expression

$$\frac{\Gamma_{\hat{\mathbf{n}}}(\mathbf{r}, \omega)}{\Gamma_{\hat{\mathbf{n}}}^{0}(\omega)} = \frac{\text{LDOS}_{\hat{\mathbf{n}}}(\mathbf{r}, \omega)}{\text{LDOS}_{\hat{\mathbf{n}}}^{0}(\omega)}$$

where $\Gamma_{\hat{\mathbf{n}}}^0(\omega)$ and $LDOS_{\hat{\mathbf{n}}}^0(\omega) = \omega^2/(3\pi^2c^3)$ are the decay rate and LDOS in a vacuum, respectively. This expression applies, as well, to a classical dipole emitter, in which case $\Gamma_{\hat{\mathbf{n}}}(\mathbf{r},\omega)$ is replaced by the power radiated by the dipole. We can separate the contribution induced by the nanostructure from that of a vacuum as $LDOS_{\hat{\mathbf{n}}}^{ind}(\mathbf{r},\omega) = LDOS_{\hat{\mathbf{n}}}(\mathbf{r},\omega) - LDOS_{\hat{\mathbf{n}}}^0(\omega)$, which

is calculated from the induced part of the Green tensor $G^{ind}(\mathbf{r}, \mathbf{r}', \omega)$, using eq 1.

If all of the materials from which the nanostructure is made can be described using a local, causal, and linear dielectric function, $\mathbf{G}^{\mathrm{ind}}(\mathbf{r}, \mathbf{r}', \omega)$ has to satisfy Kramers–Kronig relations. This property can be exploited to obtain the following sum rule for the induced part of the LDOS⁴⁴ (see the Supporting Information for a detailed derivation)

$$\int_0^\infty LDOS_{\hat{\mathbf{n}}}^{ind}(\mathbf{r}, \,\omega) \,\,\mathrm{d}\omega = \frac{1}{4\pi} \mathbf{E}^{ind}(\mathbf{r}) \cdot \hat{\mathbf{n}} \tag{2}$$

Here, $\mathbf{E}^{\mathrm{ind}}(\mathbf{r})$ represents the static field (i.e., for $\omega=0$) generated at \mathbf{r} by a unit dipole located at that position due to the presence of the nanostructure. Notice that this field corresponds only to the component induced through the nanostructure at the dipole position, and, hence, it does not include the bare dipole field, which would diverge at that position. The sum rule given in eq 2, thus, bounds the spectral integral of the induced LDOS by the field of a static dipole.

We begin by examining the validity of the sum rule with a simple nanostructure, namely, a spherical metallic nanoparticle of radius R, as shown in Figure 1(a). A unit dipole is placed a

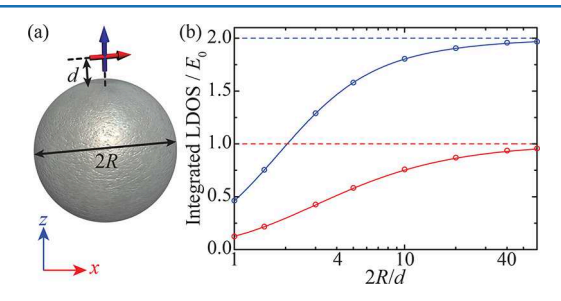


Figure 1. (a) Schematics of a spherical nanoparticle of radius R with a dipole placed a distance d above its surface, which points along the x (red) or z (blue) axis. (b) Comparison between the integral of the induced LDOS (circles) and the field of a static dipole (solid curves) as a function of the dimensionless parameter 2R/d. The dashed curves represent the field of a static dipole placed in front of a perfectly conducting planar surface. All quantities are normalized to $E_0 = 1/(32\pi d^3)$.

distance d above its surface, oriented along either the x (red) or z (blue) axis, indicating the point at which we analyze the sum rule. Notice that by analyzing these two directions we cover all possible orientations. We model the material from which the nanosphere is made using a Drude dielectric function:

$$\varepsilon_{\rm D}(\omega) = 1 - \frac{\omega_{\rm p}^2}{\omega(\omega + i\gamma_{\rm p})} \tag{3}$$

where $\omega_{\rm p}$ is the plasma frequency and $\gamma_{\rm p}$ represents the damping associated with the nonradiative losses of the material. Here, for simplicity, we choose $\hbar\omega_{\rm p}=4$ eV and $\gamma_{\rm p}=0.01\omega_{\rm p}$. Under these conditions, at $\omega=0$ the dielectric function diverges, which means that the nanostructure behaves as a perfect conductor. Therefore, the static field in the right-hand side of eq 2 can be calculated analytically using the method of images, ⁴⁶ as detailed in the Supporting Information. On the other hand, the spherical symmetry of the nanostructure allows us to calculate the induced LDOS using Mie theory, ⁴⁷ through an expansion of the electromagnetic field in terms of multipolar waves.

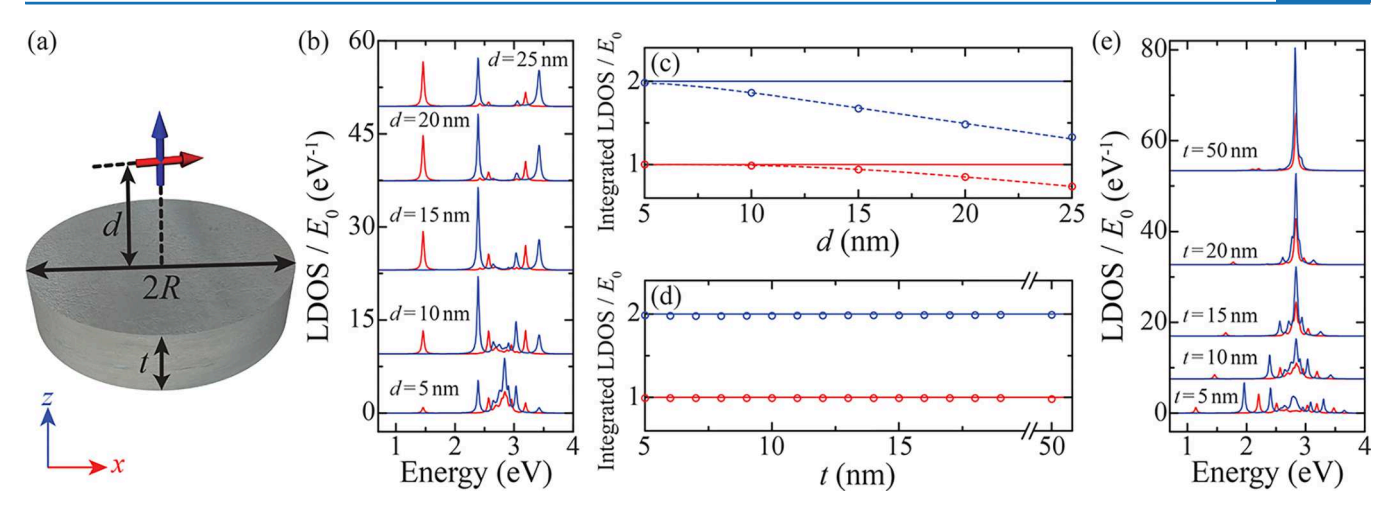


Figure 2. (a) Schematics of a nanodisk of radius R and thickness t with a dipole placed a distance d above its surface pointing along the x (red) or z (blue) axis. (b) Induced LDOS spectrum for a disk with R=25 nm and t=10 nm, calculated at different distances, as indicated by the labels. (c) Integral of the induced LDOS (circles) for the distances discussed in panel (a) and the corresponding induced field generated by a static dipole calculated either numerically (dashed curves) or using the method of images (solid curves). (d) Integral of the induced LDOS (circles) as a function of the nanodisk thickness and corresponding induced field generated by a static dipole, obtained using the method of images (solid curves). (e) Induced LDOS spectrum for a disk with R=25 nm calculated at d=5 nm for different values of t.

Figure 1(b) shows the comparison between the integrated induced LDOS (circles) and the field of a static dipole (solid curves), plotted as a function of the dimensionless parameter 2R/d. Here and in the rest of the paper, we normalize all results to $E_0 = 1/(32\pi d^3)$, which is $1/4\pi$ times the field induced by a static dipole placed parallel to, and a distance d from, a perfectly conducting planar surface. Examining the results of panel (b), we observe that the sum rule is fulfilled in the entire range of geometries considered, with an error of the same order of magnitude as the numerical precision of our simulations. As 2R/d grows, the nanosphere locally approaches an infinite planar surface, and therefore both sides of the sum rule converge to E_0 , for the x case, and $2E_0$, for the z one (see Supporting Information), as indicated by the red and blue dashed curves, respectively.

The simplicity of the nanosphere makes it a good initial example, but, at the same time, it prevents us from exploring the effect that the aspect ratio of the nanostructure has on the sum rule. To circumvent this, we analyze the sum rule for a metallic nanodisk of radius R = 25 nm and thickness t_1 , which is shown in Figure 2(a). We describe its material properties using the same Drude dielectric function as for the nanosphere. Due to the lack of spherical symmetry, Mie theory is no longer applicable, so we calculate the induced LDOS through the full numerical solution of Maxwell's equations using the boundary element method (BEM). Figure 2(b) displays the results of this calculation for five different distances d above the surface of the disk, ranging from 5 to 25 nm. These spectra show different resonances, whose height is modified as d is varied, corresponding to the different plasmonic modes supported by the nanodisk. For instance, the resonance at ~1.5 eV, which only appears in the x case (red curves), corresponds to a dipolar plasmon. The radiative character of this mode makes its excitation less efficient as the distance decreases. This is also the case for the mode appearing at \sim 2.4 eV for the z case (blue curve). On the other hand, the resonances located around 2.8 eV are clearly nonradiative, since they disappear as d is increased. Indeed, they correspond to the surface plasmon of a planar surface, which appears at $\omega \approx \omega_{\rm p}/\sqrt{2}$, and is split into

multiple resonances due to the interaction between the upper and lower surfaces of the disk.

We verify the validity of the sum rule by plotting the integrated spectra of panel (b) alongside the corresponding induced field generated by a static dipole. These results are shown in panel (c) using respectively circles and dashed curves. The static field is calculated using BEM since, due to the lack of symmetry of the nanodisks, the method of images is not convenient in this case. Comparing these two sets of results, we confirm the validity of the sum rule for all the distances under consideration. Expectedly, as d/R decreases, the static field (and hence the integrated LDOS) approaches that of a perfectly conducting planar surface, namely, E_0 for the x case and $2E_0$ for the z case, which are indicated by the solid curves. This means that, within this limit, the right-hand side of eq 2 only depends on d and not on the radius or the thickness of the nanodisk, as confirmed by the results shown in panel (d). There, we plot the integral of the induced LDOS (circles) and the corresponding static field, obtained with the method of images, as a function of the disk thickness. It is important to remark that, although the integrated LDOS does not vary with t, the corresponding spectrum is strongly dependent on it. This can be seen in panel (e), where we plot the induced LDOS spectra for d = 5 nm and different nanodisk thicknesses, ranging from 5 to 50 nm. For small t, the spectrum displays multiple resonances around $\hbar\omega_{
m p}/$ $\sqrt{2} \approx 2.8$ eV, which, as discussed before, arise from the interaction between the surface plasmons of the upper and lower plates of the nanodisk. As the thickness increases, the coupling between the modes of the two plates decreases, and the resonances coalesce to a single peak. Since the area under the spectrum is fixed by the sum rule, the reduction of the number of peaks is compensated by an increase in their height, as clearly seen in panel (e).

A similar behavior is expected if, instead of changing t, we modify the shape of the nanostructure, keeping $d/R \ll 1$. To corroborate this prediction, we investigate the induced LDOS for three different nanostructures: a nanodisk of radius R=25 nm, a nanosquare of side length 2R=50 nm, and an equilateral nanotriangle of height 3R=75 nm. In all cases, we calculate the induced LDOS at a point located a distance d=5 nm above the

center of the nanostructure, as indicated in Figure 3(a). The resulting spectra are plotted in panels (b) and (c) for t = 5 and t

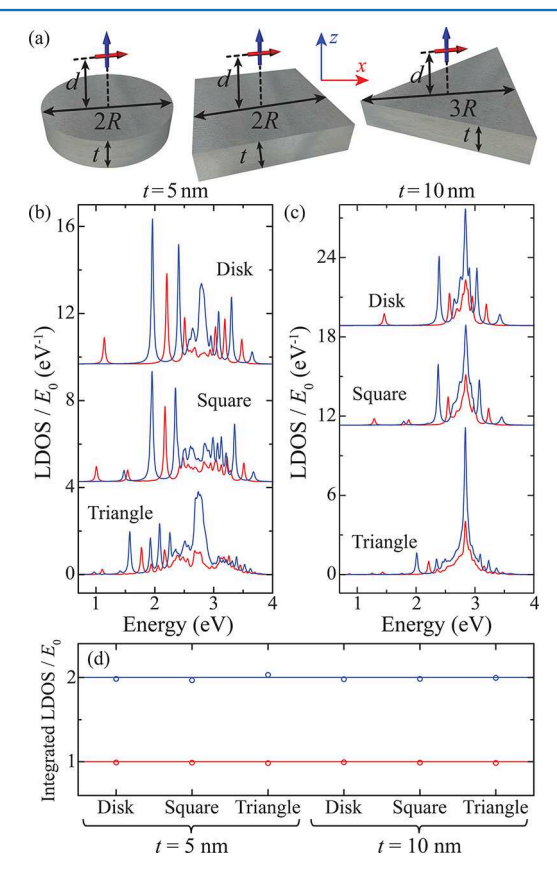


Figure 3. (a) Schematics of three nanostructures with equal thicknesses t and different shapes: a nanodisk of radius R=25 nm, a nanosquare of side length 2R=50 nm, and an equilateral nanotriangle of height 3R=75 nm. In all cases, a unit dipole is placed a distance d=5 nm above their surfaces pointing along the x (red) or z (blue) axis. (b, c) Induced LDOS spectra for the three nanostructures of panel (a) with thicknesses t=5 (b) and t=10 nm (c). (d) Integral of the induced LDOS (circles) compared with the induced field of a static dipole (solid curves), calculated using the method of images for a perfectly conducting planar surface.

= 10 nm, respectively. Clearly, the shape of the nanostructure has a major impact on the induced LDOS spectra, dictating the number of resonances, as well as their spectral positions and heights. However, as shown in panel (d), the integral of the induced LDOS (circles) remains the same for all of the geometries, being equal to E_0 in the x case (red curve) and $2E_0$ in the z one (blue curve). These results highlight how the sum rule investigated here can be used as a guide to select the most favorable geometries to enhance the decay rate of an emitter placed near the surface of a nanostructure.

It is important to notice that, as long as the nanostructure is made of a metallic material (i.e., it has at least one free electron), it behaves as a perfect conductor at $\omega=0$. This means that, for a given geometry, the integral of the induced LDOS is independent of the parameters of the Drude dielectric function ω_p and γ_p , although the spectrum itself does depend on them. This is demonstrated in panels (a) and (d) of Figure 4 for a nanodisk with R=25 nm, t=10 nm, at a point located a distance d=5 nm above its surface. Specifically, panel (a) shows the induced LDOS spectrum for three different values of $\hbar\omega_p$, with $\hbar\gamma_p$ fixed to 0.04 eV. Expectedly, as ω_p grows, the

LDOS spectrum blue-shifts. However, its area remains unchanged, as shown in panel (d) by the circles, and equals the corresponding induced static field (solid curves), calculated using the method of images for a perfectly conducting planar surface. As always, red and blue colors are used to indicate the x and z cases, respectively.

So far, we have restricted ourselves to nanostructures made of an ideal metal, whose material properties are described using a pure Drude dielectric function. However, real metals such as gold and silver have more complicated dielectric responses, arising from effects that are neglected in the Drude description, such as interband transitions. It is possible, however, to describe the effect of these interband transitions by adding Lorentzian terms into the Drude dielectric function, $\varepsilon_{\rm D}(\omega)$, given in eq 3. This results in the so-called Drude–Lorentz dielectric function: 46,53

$$\varepsilon_{\rm DL}(\omega) = \varepsilon_{\rm D}(\omega) + \frac{A}{{\omega_0}^2 - (\omega + i\gamma_0/2)^2}$$

where A quantifies the strength of the transition, ω_0 is the transition frequency, and γ_0 is the associated damping. To explore the effect that the addition of the Lorentz term has on the sum rule, we investigate the same nanodisk as in panel (a) but now made of a material described with $arepsilon_{
m DL}(\omega)$. In particular, we choose $\hbar\omega_{\rm p}=4$ eV, $\hbar\gamma_{\rm p}=0.04$ eV, $\hbar\omega_{\rm 0}=3$ eV, and $\hbar \gamma_0 = 0.16$ eV. Figure 4(b) shows the evolution of the induced LDOS spectrum for the different values of A indicated by the labels. As the value of A grows, the height of the resonances in the spectrum decrease, but, at the same time, the resonances become broader. This is consistent with the fact that the area under the spectrum has to remain invariant since, despite the addition of the Lorentz term, at $\omega = 0$, the material still behaves as a perfect conductor, and, consequently, the static field remains equal to that of a perfectly conducting planar surface. This can be seen in panel (e), where we compare the integral of the induced LDOS (circles) and the static field (solid curves) as a function of A.

The Drude-Lorentz dielectric function can also be used to model dielectric materials by taking $\omega_{
m p}$ = 0. In this case, at ω = 0, the material does not behave as a perfect conductor since it does not have any free electrons. Therefore, the static field is now dependent on the dielectric function. In particular, for a planar surface, the method of images results in a extra factor of $A/(A + 2(\omega_0^2 + \gamma_0^2/4))$, multiplying the result for a perfect conductor (see the Supporting Information). This means that, if we repeat the calculations of panel (b) taking $\omega_{\rm p}$ = 0, the area under the induced LDOS spectrum must vary with A. This is clearly shown in Figure 4(c), where we plot the induced LDOS spectrum for three different values of A. In fact, the integral of the induced LDOS, plotted with circles in panel (f), grows linearly with A, as expected from the factor $A/(A + 2(\omega_0^2 + \gamma_0^2))$ 4)), which, for $A \ll \omega_0^2$, reduces to $A/(2\omega_0^2)$. Incidentally, in this case, the agreement of the integrated LDOS and the static field calculated with the method of images (solid curves) is not as good as in previous examples. We attribute this to the less efficient screening of bound electrons as compared with that of the free electrons, which results in the edges of the nanostructure having a noticeable contribution to the static field. However, if we calculate the latter using BEM (dashed curves), the agreement with the integrated LDOS is recovered, as required by the sum rule. These examples demonstrate how the investigated sum rule can help to understand the limits of

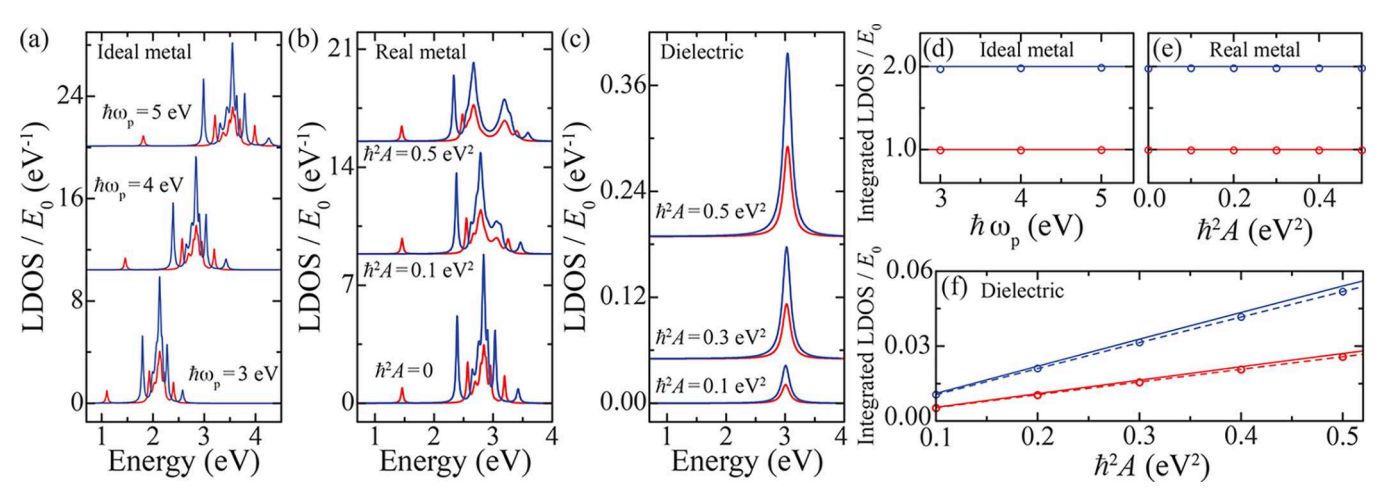


Figure 4. (a–c) Induced LDOS spectrum evaluated at d=5 nm above the surface of a nanodisk with R=25 nm, t=10 nm, made of different materials. (a) Nanodisk made of an ideal metal described using a Drude dielectric function with $\hbar\gamma_p=0.04$ eV and different values of $\hbar\omega_p$. (b) Nanodisk made of a real metal described with a Drude–Lorentz dielectric function with $\hbar\omega_p=4$ eV, $\hbar\gamma_p=0.04$ eV, $\hbar\omega_0=3$ eV, $\hbar\gamma_0=0.16$ eV, and different values of A. (c) Nanodisk made of a dielectric material described using a Drude–Lorentz dielectric function with vanishing ω_p , $\hbar\omega_0=3$ eV, $\hbar\gamma_0=0.16$ eV, and different values of A. (d–f) Comparison between the integral of the induced LDOS (circles) and the static field for the nanodisks analyzed in panels (a), (b), and (c), respectively. Solid curves represent the results of the static field calculated using the method of images for a perfectly conducting planar surface, while dashed curves are used to indicate the calculations performed with BEM. In all cases, red and blue colors correspond respectively to the x and z cases, as indicated in Figure 2(a).

the LDOS produced by structures made of different types of materials.

Although we have focused so far on finite nanostructures, the sum rule under investigation applies equally to extended systems, such as metallic slabs. In these cases, thanks to the translational invariance of the system, we can compute the induced LDOS analytically, as explained in the Supporting Information. Furthermore, the right-hand side of the sum rule can be obtained exactly by using the method of images for a perfectly conducting planar surface. As a first example, we investigate the metal slab of thickness t shown in Figure 5(a). We describe the material properties of the structure using a Drude dielectric response with $\hbar\omega_{\rm p}=4$ eV and $\gamma_{\rm p}=0.01\omega_{\rm p}$. The corresponding induced LDOS spectrum is plotted in panel (c) for different values of d and t. As expected, smaller values of t result in the hybridization of the surface plasmon supported at the upper and lower surfaces, which leads to a splitting of the resonance. This splitting disappears when t is increased, leaving a much stronger and narrower resonance (notice the different scales in the upper and lower parts of the plot). The LDOS spectrum also depends on d; in particular, for small distances, the contribution of large wave vectors, outside the light cone, becomes stronger, which results in a smaller splitting. However, despite the changes in the LDOS spectra, the corresponding integrals for each value of d always have to be the same. This is confirmed in Figure 5(d), where we compare the static field (solid curves) with the integral of the induced LDOS (circles).

To complete our analysis of extended systems, we also investigate the case of a pure two-dimensional material, namely, a graphene sheet, which is depicted in Figure 5(b). This material, when doped, behaves as a metal, with a surface conductivity that can be modeled within the random phase approximation, at temperature T = 0 K, using 54

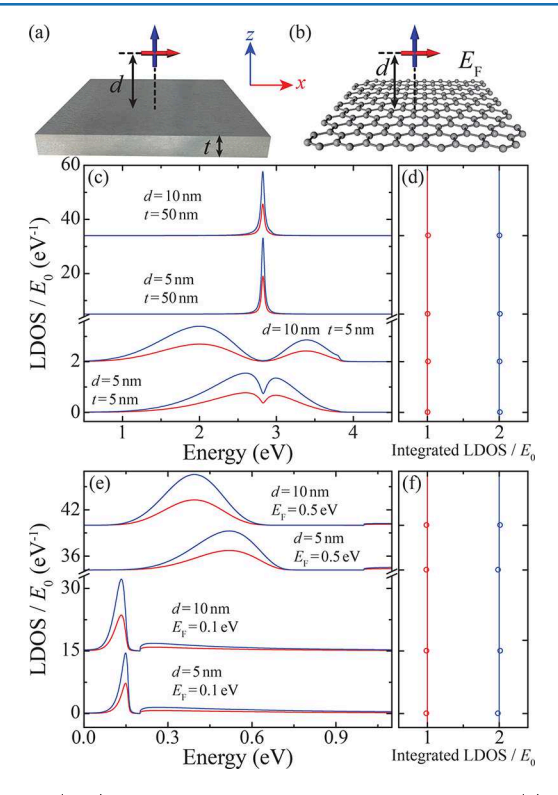


Figure 5. (a, b) Schematics of a metallic slab of thickness t (a) and a graphene sheet with Fermi energy $E_{\rm F}$ (b). In both cases, a dipole is placed a distance d from the surface oriented along the x (red) or z (blue) axis. (c) Induced LDOS spectrum for the metallic slab calculated for different values of t and d. (d) Comparison between the integral of the induced LDOS (circles) and the corresponding static field (solid curves) for the structures analyzed in panel (c). (e, f) Same as (c, d), but for the graphene sheet with different values of d and $E_{\rm F}$.

$$\sigma(\omega) = \frac{ie^2}{\pi\hbar^2} \frac{E_F}{\omega + i\gamma} + \frac{e^2}{4\hbar} \left[\theta(\hbar\omega - 2E_F) + \frac{i}{\pi} \log \left| \frac{\hbar\omega - 2E_F}{\hbar\omega + 2E_F} \right| \right]$$

Here, $\theta(x)$ is a step function and $E_{\rm F}$ is the Fermi energy, which determines the level of doping of the graphene sheet. Furthermore, γ is the damping rate given by $\gamma = e v_{\rm F}^2/(\mu E_{\rm F})$ in terms of the Fermi velocity $v_{\rm F} \approx c/300$ and the electron mobility μ , for which we assume a value of 10^4 cm $^2/({\rm V~s})$. Although this expression of the conductivity is strictly valid at T=0 K and for $\gamma=0$, it is a very good approximation for Fermi energies larger than the thermal energy $k_{\rm B}T$, which, at room temperature, is ~ 0.026 eV.

Using this surface conductivity, we can calculate the induced LDOS spectrum at distance d from the graphene sheet. The corresponding results are plotted in Figure 5(e) for different values of d and $E_{\rm E}$. In all cases, we observe a single resonance, corresponding to the surface plasmon supported by the graphene sheet, which blue-shifts, becomes broader, and reduces its height (notice the different scales in the upper and lower parts of the plot) as E_F increases. A sharp feature is visible at $\hbar\omega = 2E_{\rm F}$, corresponding to the threshold of interband transitions (second term in the surface conductivity), which adds a nonradiative contribution to the LDOS. The sum rule is satisfied in each of these cases, as shown in Figure 5(f), where we compare the integral of the induced LDOS (circles) with the field induced by a static dipole (solid curves). These results confirm that the integral of the induced LDOS, evaluated at a certain distance from a planar metallic structure, is always independent of its thickness, as well as of its material properties, as long as the system remains metallic. More broadly, the presented analysis can help to understand the interaction of emitters with substrates, which is a relevant problem for applications in sensing and photochemistry.

The derivation of the sum rule for the induced LDOS can be generalized to obtain a sum rule for the cross density of states. This quantity measures the intrinsic spatial coherence of the electric field near a nanostructure.^{31,55,56} Furthermore, it is proportional to the so-called cross-decay rate of two dipole emitters interacting in the presence of a nanostructure.^{45,57–59} Similar to the LDOS, the CDOS is obtained from the Green tensor, evaluated, in this case, at two different positions:

$$CDOS_{\hat{\mathbf{n}},\hat{\mathbf{n}}'}(\mathbf{r}, \mathbf{r}', \omega) = -\frac{2\omega}{\pi} Im\{\hat{\mathbf{n}} \cdot \mathbf{G}(\mathbf{r}, \mathbf{r}', \omega) \cdot \hat{\mathbf{n}}'\}$$

The contribution induced by the nanostructure can be separated from that of a vacuum as $CDOS_{\hat{n},\hat{n}'}^{ind}(r, r', \omega) = CDOS_{\hat{n},\hat{n}'}(r, r', \omega) - CDOS_{\hat{n},\hat{n}'}^{0}(r, r', \omega)$, and, therefore, is proportional to the imaginary part of $G^{ind}(r, r', \omega)$. As detailed in the Supporting Information, we can follow the same procedure as in the derivation of eq 2 to obtain the following sum rule for the induced CDOS:

$$\int_0^\infty \text{CDOS}_{\hat{\mathbf{n}},\hat{\mathbf{n}}'}^{\text{ind}}(\mathbf{r},\mathbf{r}',\omega) d\omega = \frac{1}{4\pi} \mathbf{E}^{\text{ind}}(\mathbf{r};\mathbf{r}',\hat{\mathbf{n}}') \cdot \hat{\mathbf{n}}$$
(4)

where $E^{ind}(\mathbf{r}; \mathbf{r}', \hat{\mathbf{n}}')$ is the field created at \mathbf{r} , by a static dipole located at \mathbf{r}' , oriented along $\hat{\mathbf{n}}'$.

To confirm the validity of this sum rule, we analyze the case of a metallic nanosphere of radius R = 25 nm with two dipoles placed a distance d = 15 nm above its surface, separated by an

angle θ , as shown in Figure 6(a). The material properties of the nanostructure are described using a Drude dielectric function

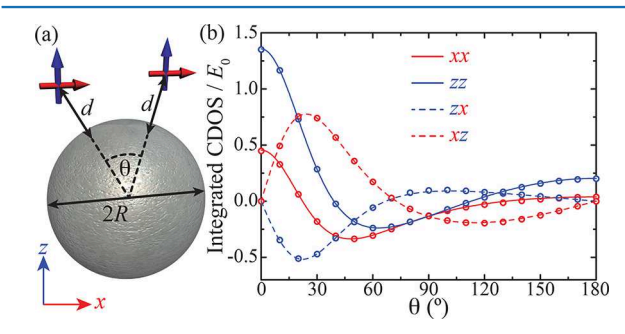


Figure 6. (a) Schematics of a nanoparticle of radius R=25 nm with two dipoles placed a distance d=15 nm from its surface separated by an angle θ . Each of the dipoles is oriented along either the x (red) or z (blue) axis. (b) Comparison, as a function of θ , of the integral of the induced CDOS (circles) and the corresponding static field induced by the left dipole at the position of the right one (curves). We analyze four possible combinations of the relative orientation of the two dipoles, as indicated in the legend by xx, zz, zx, and xz, where the first (second) letter corresponds to the orientation of the right (left) dipole.

with $\hbar\omega_{\rm p}=4~{\rm eV}$ and $\gamma_{\rm p}=0.01\omega_{\rm p}$. We calculate the static field induced by the left dipole at the position of the one placed on the right as a function of θ using the method of images for a spherical geometry (see the Supporting Information). The corresponding results are plotted in Figure 6(b) for four different combinations of the orientation of the dipoles: xx, zz, zx, and xz, where the first (second) letter in these labels indicates the orientation of the right (left) dipole (see the legend). We compare the static field with the integral of the induced CDOS, calculated using Mie theory, which is plotted using circles. As expected, the two sets of calculations are in excellent agreement for all values of θ under consideration. At $\theta=0^\circ$ and $\theta=180^\circ$, the xz and zx cases vanish due to the symmetry of the induced field. Indeed, for $\theta=0^\circ$ the induced CDOS reduces to the induced LDOS.

The CDOS sum rule applies, as well, to extended systems. In order to verify it, we consider the case of a metallic slab of thickness t with two dipoles placed a distance d = 10 nm above its surface, separated by D = 20 nm, as shown in Figure 7(a). We describe the material properties of the slab using a Drude dielectric response with $\hbar\omega_{\rm p}=4$ eV and $\gamma_{\rm p}=0.01\omega_{\rm p}$. The corresponding induced CDOS spectrum is plotted in Figure 7(b) for t = 50 nm (upper curves) and t = 5 nm (lower curves). We investigate three different combinations of the orientation of the dipoles—xx, zz, and xz—where the first (second) letter in these labels indicates the orientation of the right (left) dipole (see the legend). Notice that, in this case, the zx combination produces the same result as the xz but with opposite sign. Examining the results, we observe that, as it was in the case of the LDOS, the thinner slab presents a spectrum with more features than the thicker one, which we attribute to the stronger hybridization between the surface plasmon supported at the upper and lower surfaces of the structure. Due to the fixed value of the integrated CDOS, a larger number of features in the spectrum has to come associated with smaller peak values (notice the different scales in the upper and lower parts of the plot). The validity of the CDOS sum rule is confirmed in panel (c), where we compare, as a function of the thickness of the slab, the integrated CDOS (circles) with the static field induced

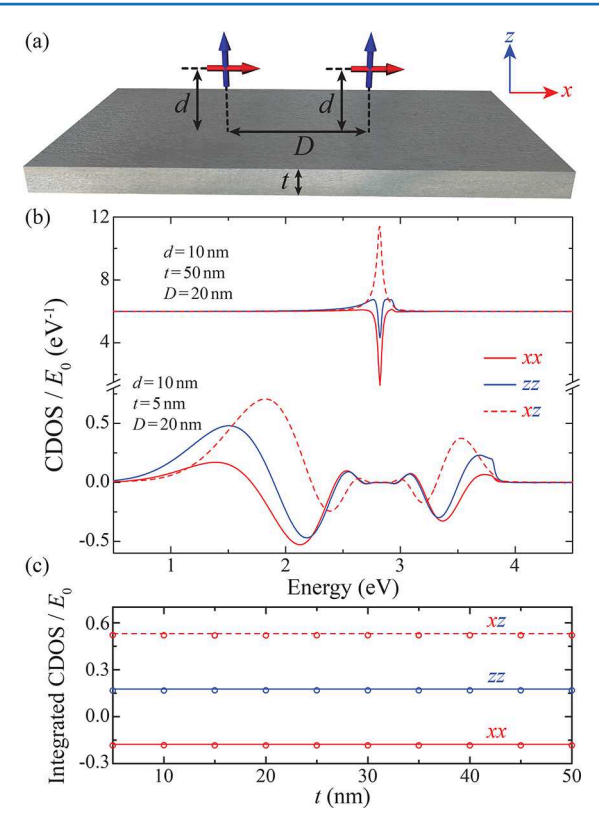


Figure 7. (a) Schematics of a metallic slab of thickness t with two dipoles located a distance d=10 nm above it and separated from each other by D=20 nm. Each of the dipoles is oriented along either the x (red) or z (blue) axis. (b) Induced CDOS spectrum for t=50 nm (upper curves) and t=5 nm (lower curves). (c) Comparison, as a function of t, of the integral of the induced CDOS (circles) and the corresponding static field induced by the left dipole at the position of the right one (curves). We analyze three possible combinations of the relative orientation of the two dipoles, as indicated in the legend by xx, zz, and xz, where the first (second) letter corresponds to the orientation of the right (left) dipole.

by the left dipole at the position of the right one (curves). The latter is calculated using the method of images (see Supporting Information). These results show the potential of the analyzed CDOS sum rule to guide the design of nanostructures capable of enhancing the coupling between dipole emitters placed in their vicinity.

CONCLUSIONS

In summary, we have investigated the response of different nanostructures to near-field excitation by dipole emitters through the analysis of a sum rule for the induced LDOS. This relation bounds the spectral integral of the LDOS induced by a nanostructure to the field generated by a static dipole in its presence. We have verified the sum rule for a wide variety of systems including finite nanostructures such as nanospheres, nanodisks, nanotriangles, and nanosquares, made of metallic as well as dielectric materials. We have also shown that it applies to extended systems, such as metal films and graphene sheets. Through this study, we have shown that the spectral integral of the LDOS near metallic nanostructures is independent of the material parameters, such as the plasma frequency and the damping. We have shown, as well, that this quantity is independent of the thickness for metallic slabs and of the Fermi level of graphene sheets. Although we have focused on the

electric part of the LDOS, the sum rule investigated here can be directly extended to the magnetic component of LDOS, ^{27,31} which governs the decay rate of magnetic dipole transitions. ^{60,61} Furthermore, we have applied the sum rule to the CDOS, a quantity that measures the spatial coherence of the electric field near a nanostructure and determines the interaction between two dipoles in its presence. Our work serves to highlight the usefulness of the analyzed sum rule in the understanding of the limits of the near-field response of nanostructures, and shows how to exploit it as a tool to guide the selection of the most favorable nanostructure geometries and materials for achieving strong values of the LDOS and the CDOS over desired parts of the spectrum.

ASSOCIATED CONTENT

S Supporting Information

The Supporting Information is available free of charge on the ACS Publications website at DOI: 10.1021/acsphotonics.8b00225.

Derivation of the sum rule for the LDOS and CDOS; outline of the method of images for a dipole placed in front of a plane and a sphere; derivation of the induced LDOS and CDOS near a planar system (PDF)

AUTHOR INFORMATION

Corresponding Author

*E-mail: manjavacas@unm.edu.

ORCID 6

Alejandro Manjavacas: 0000-0002-2379-1242

Notes

The authors declare no competing financial interest.

ACKNOWLEDGMENTS

This work has been sponsored by the U.S. National Science Foundation (Grant ECCS-1710697). We also acknowledge the UNM Center for Advanced Research Computing for computational resources used in this work.

■ REFERENCES

- (1) Novotny, L.; Hecht, B. Principles of Nano-Optics; Cambridge University Press: New York, 2006.
- (2) Atwater, H. A.; Polman, A. Plasmonics for improved photovoltaic devices. *Nat. Mater.* **2010**, *9*, 205–213.
- (3) Baffou, G.; Quidant, R. Nanoplasmonics for Chemistry. Chem. Soc. Rev. 2014, 43, 3898-3907.
- (4) Brongersma, M. L.; Halas, N. J.; Nordlander, P. Plasmon-induced hot carrier science and technology. *Nat. Nanotechnol.* **2015**, *10*, 25–34.
- (5) Johansson, P.; Xu, H.; Käll, M. Surface-enhanced Raman scattering and fluorescence near metal nanoparticles. *Phys. Rev. B: Condens. Matter Mater. Phys.* **2005**, 72, 035427.
- (6) Moskovits, M. Surface-enhanced Raman spectroscopy: a brief retrospective. J. Raman Spectrosc. 2005, 36, 485-496.
- (7) Lozano, G.; Louwers, D. J.; Rodriguez, S. R. K.; Murai, S.; Jansen, O. T. A.; Verschuuren, M. A.; Gomez Rivas, J. Plasmonics for solid-state lighting: enhanced excitation and directional emission of highly efficient light sources. *Light: Sci. Appl.* **2013**, *2*, e241.
- (8) Yang, A.; Odom, T. W. Breakthroughs in Photonics 2014: Advances in Plasmonic Nanolasers. *IEEE Photonics J.* **2015**, *7*, 1–6.
- (9) Naik, G. V.; Shalaev, V. M.; Boltasseva, A. Alternative Plasmonic Materials: Beyond Gold and Silver. Adv. Mater. 2013, 25, 3264-3294.
- (10) Myroshnychenko, V.; Carbó-Argibay, E.; Pastoriza-Santos, I.; Pérez-Juste, J.; Liz-Marzán, L. M.; García de Abajo, F. J. Modelling the optical response of highly faceted metal nanoparticles with a fully 3D boundary element method. *Adv. Mater.* 2008, 20, 4288–4293.

(11) Miller, O. D.; Polimeridis, A. G.; Reid, M. T. H.; Hsu, C. W.; DeLacy, B. G.; Joannopoulos, J. D.; Soljačić, M.; Johnson, S. G. Fundamental limits to optical response in absorptive systems. *Opt. Express* **2016**, *24*, 3329–3364.

- (12) Miller, O. D.; Hsu, C. W.; Reid, M. T. H.; Qiu, W.; DeLacy, B. G.; Joannopoulos, J. D.; Soljačić, M.; Johnson, S. G. Fundamental limits to extinction by metallic nanoparticles. *Phys. Rev. Lett.* **2014**, *112*, 123903.
- (13) Sohl, C.; Gustafsson, M.; Kristensson, G. Physical limitations on broadband scattering by heterogeneous obstacles. *J. Phys. A: Math. Theor.* **2007**, *40*, 11165.
- (14) Sohl, C.; Gustafsson, M.; Kristensson, G. Physical limitations on metamaterials: restrictions on scattering and absorption over a frequency interval. *J. Phys. D: Appl. Phys.* **2007**, 40, 7146.
- (15) Raman, A.; Shin, W.; Fan, S. Upper Bound on the Modal Material Loss Rate in Plasmonic and Metamaterial Systems. *Phys. Rev. Lett.* **2013**, *110*, 183901.
- (16) Hugonin, J.-P.; Besbes, M.; Ben-Abdallah, P. Fundamental limits for light absorption and scattering induced by cooperative electromagnetic interactions. *Phys. Rev. B: Condens. Matter Mater. Phys.* **2015**, 91, 180202.
- (17) Miller, O. D.; Ilic, O.; Christensen, T.; Reid, M. T. H.; Atwater, H. A.; Joannopoulos, J. D.; Soljačić, M.; Johnson, S. G. Limits to the Optical Response of Graphene and Two-Dimensional Materials. *Nano Lett.* **2017**, *17*, 5408–5415.
- (18) Altarelli, M.; Dexter, D. L.; Nussenzveig, H. M.; Smith, D. Y. Superconvergence and Sum Rules for the Optical Constants. *Phys. Rev. B* **1972**, *6*, 4502–4509.
- (19) King, F. W. Sum rules for the optical constants. J. Math. Phys. 1976, 17, 1509-1514.
- (20) Forcella, D.; Prada, C.; Carminati, R. Causality, Nonlocality, and Negative Refraction. *Phys. Rev. Lett.* **2017**, *118*, 134301.
- (21) Carminati, R.; Sáenz, J. J. Density of States and Extinction Mean Free Path of Waves in Random Media: Dispersion Relations and Sum Rules. *Phys. Rev. Lett.* **2009**, *102*, 093902.
- (22) Kuhn, W. Über die Gesamtstärke der von einem Zustande ausgehenden Absorptionslinien. Eur. Phys. J. A 1925, 33, 408-412.
- (23) Reiche, F.; Thomas, W. Über die Zahl der Dispersionselektronen, die einem stationären Zustand zugeordnet sind. Eur. Phys. J. A 1925, 34, 510–525.
- (24) Barnett, S. M.; Loudon, R. Optical Thomas-Reiche-Kuhn Sum Rules. *Phys. Rev. Lett.* **2012**, *108*, 013601.
- (25) Sievers, A. J. Extinction sum rule and optical moment for an ellipsoid particle of arbitrary shape. *Opt. Commun.* **1994**, *109*, 71–74.
- (26) Yang, Z.-J.; Antosiewicz, T. J.; Verre, R.; García de Abajo, F. J.; Apell, S. P.; Käll, M. Ultimate limit of light extinction by nanophotonic structures. *Nano Lett.* **2015**, *15*, 7633–7638.
- (27) Joulain, K.; Carminati, R.; Mulet, J. P.; Greffet, J. J. Definition and measurement of the local density of electromagnetic states close to an interface. *Phys. Rev. B: Condens. Matter Mater. Phys.* **2003**, 68, 245405
- (28) Fussell, D. P.; McPhedran, R. C.; Martijn de Sterke, C. Three-dimensional Green's tensor, local density of states, and spontaneous emission in finite two-dimensional photonic crystals composed of cylinders. *Phys. Rev. E* **2004**, *70*, 066608.
- (29) Kuttge, M.; Vesseur, E. J. R.; Koenderink, A. F.; Lezec, H. J.; Atwater, H. A.; García de Abajo, F. J.; Polman, A. Local density of states, spectrum, and far-field interference of surface plasmon polaritons probed by cathodoluminescence. *Phys. Rev. B: Condens. Matter Mater. Phys.* 2009, 79, 113405.
- (30) Krachmalnicoff, V.; Castanié, E.; De Wilde, Y.; Carminati, R. Fluctuations of the Local Density of States Probe Localized Surface Plasmons on Disordered Metal Films. *Phys. Rev. Lett.* **2010**, *105*, 183901
- (31) Carminati, R.; Cazé, A.; Cao, D.; Peragut, F.; Krachmalnicoff, V.; Pierrat, R.; Wilde, Y. D. Electromagnetic density of states in complex plasmonic systems. *Surf. Sci. Rep.* **2015**, *70*, 1–41.
- (32) Shahbazyan, T. V. Local Density of States for Nanoplasmonics. *Phys. Rev. Lett.* **2016**, *117*, 207401.

(33) Dereux, A.; Girard, C.; Weeber, J.-C. Theoretical principles of near-field optical microscopies and spectroscopies. *J. Chem. Phys.* **2000**, 112, 7775–7789.

- (34) Purcell, E. M. Spontaneous emission probabilities at radio frequencies. *Phys. Rev.* **1946**, *69*, *681*.
- (35) Barnett, S. M.; Huttner, B.; Loudon, R. Spontaneous emission in absorbing dielectric media. *Phys. Rev. Lett.* **1992**, *68*, 3698–3701.
- (36) Noginov, M. A.; Li, H.; Barnakov, Y. A.; Dryden, D.; Nataraj, G.; Zhu, G.; Bonner, C. E.; Mayy, M.; Jacob, Z.; Narimanov, E. E. Controlling spontaneous emission with metamaterials. *Opt. Lett.* **2010**, 35, 1863–1865.
- (37) Poddubny, A. N.; Belov, P. A.; Ginzburg, P.; Zayats, A. V.; Kivshar, Y. S. Microscopic model of Purcell enhancement in hyperbolic metamaterials. *Phys. Rev. B: Condens. Matter Mater. Phys.* **2012**, *86*, 035148.
- (38) Sauvan, C.; Hugonin, J. P.; Maksymov, I. S.; Lalanne, P. Theory of the Spontaneous Optical Emission of Nanosize Photonic and Plasmon Resonators. *Phys. Rev. Lett.* **2013**, *110*, 237401.
- (39) Carminati, R.; Greffet, J.-J.; Henkel, C.; Vigoureux, J. Radiative and non-radiative decay of a single molecule close to a metallic nanoparticle. *Opt. Commun.* **2006**, *261*, 368–375.
- (40) Barnett, S. M.; Loudon, R. Sum rule for modified spontaneous emission rates. *Phys. Rev. Lett.* **1996**, *77*, 2444–2446.
- (41) Barnett, S. M.; Loudon, R. Sum rule for environmentally modified spontaneous emission rates. *Quantum Semiclassical Opt.* **1998**, *10*, 591.
- (42) Scheel, S. Sum rule for local densities of states in absorbing dielectrics. *Phys. Rev. A: At., Mol., Opt. Phys.* **2008**, 78, 013841.
- (43) Cao, D.; Cazé, A.; Calabrese, M.; Pierrat, R.; Bardou, N.; Collin, S.; Carminati, R.; Krachmalnicoff, V.; De Wilde, Y. Mapping the Radiative and the Apparent Nonradiative Local Density of States in the Near Field of a Metallic Nanoantenna. ACS Photonics 2015, 2, 189–193.
- (44) Blum, C.; Zijlstra, N.; Lagendijk, A.; Wubs, M.; Mosk, A. P.; Subramaniam, V.; Vos, W. L. Nanophotonic Control of the Förster Resonance Energy Transfer Efficiency. *Phys. Rev. Lett.* **2012**, *109*, 203601.
- (45) Ficek, Z.; Tanaś, R. Entangled states and collective nonclassical effects in two-atom systems. *Phys. Rep.* **2002**, *372*, 369–443.
- (46) Jackson, J. D. Classical Electrodynamics; Wiley: New York, 1999.
- (47) Bohren, C. F.; Huffman, D. R. Absorption and Scattering of Light by Small Particles; Wiley-Interscience: New York, 1983.
- (48) García de Abajo, F. J.; Howie, A. Relativistic electron energy loss and electron-induced photon emission in inhomogeneous dielectrics. *Phys. Rev. Lett.* **1998**, *80*, 5180–5183.
- (49) García de Abajo, F. J.; Howie, A. Retarded field calculation of electron energy loss in inhomogeneous dielectrics. *Phys. Rev. B: Condens. Matter Mater. Phys.* **2002**, *65*, 115418.
- (50) Hohenester, U.; Trügler, A. MNPBEM A Matlab Toolbox for the simulation of plasmonic nanoparticles. *Comput. Phys. Commun.* **2012**, *183*, 370.
- (51) Waxenegger, J.; Trügler, A.; Hohenester, U. Plasmonics simulations with the MNPBEM toolbox: Consideration of substrates and layer structures. *Comput. Phys. Commun.* **2015**, *193*, 138–150.
- (52) Maier, S. A. Plasmonics: Fundamentals and Applications; Springer: New York, 2007.
- (53) Pines, D.; Nozières, P. The Theory of Quantum Liquids; W. A. Benjamin, Inc.: New York, 1966.
- (54) Koppens, F. H. L.; Chang, D. E.; García de Abajo, F. J. Graphene plasmonics: A platform for strong light-matter interactions. *Nano Lett.* **2011**, *11*, 3370–3377.
- (55) Setälä, T.; Blomstedt, K.; Kaivola, M.; Friberg, A. T. Universality of electromagnetic-field correlations within homogeneous and isotropic sources. *Phys. Rev. E: Stat. Phys., Plasmas, Fluids, Relat. Interdiscip. Top.* **2003**, 67, 026613.
- (56) Cazé, A.; Pierrat, R.; Carminati, R. Spatial Coherence in Complex Photonic and Plasmonic Systems. *Phys. Rev. Lett.* **2013**, *110*, 063903.

(57) Martín-Cano, D.; Martín-Moreno, L.; García-Vidal, F. J.; Moreno, E. Resonance Energy Transfer and Superradiance Mediated by Plasmonic Nanowaveguides. *Nano Lett.* **2010**, *10*, 3129–3134.

- (58) Gonzalez-Tudela, A.; Martin-Cano, D.; Moreno, E.; Martín-Moreno, L.; Tejedor, C.; Garcia-Vidal, F. J. Entanglement of two qubits mediated by one-dimensional plasmonic waveguides. *Phys. Rev. Lett.* **2011**, *106*, 020501.
- (59) Manjavacas, A.; Thongrattanasiri, S.; Chang, D. E.; García de Abajo, F. J. Temporal quantum control with graphene. *New J. Phys.* **2012**, *14*, 123020.
- (60) Chigrin, D. N.; Kumar, D.; Cuma, D.; von Plessen, G. Emission Quenching of Magnetic Dipole Transitions near a Metal Nanoparticle. *ACS Photonics* **2016**, *3*, 27–34.
- (61) Manjavacas, A.; Fenollosa, R.; Rodriguez, I.; Jimenez, M. C.; Miranda, M.; Meseguer, F. Magnetic Light and Forbidden Photochemistry: The Case of Singlet Oxygen. J. Mater. Chem. C 2017, 5, 11824–11831.

I

Supporting information for:

Analysis of the Limits of the Local Density of Photonic States Near Nanostructures.

Stephen Sanders and Alejandro Manjavacas*

Department of Physics and Astronomy, University of New Mexico, Albuquerque, New Mexico 87131, United States

E-mail: manjavacas@unm.edu

Sum rule derivation

We start the derivation of the sum rule by considering the following function

$$f_{\hat{\mathbf{n}},\hat{\mathbf{n}}'}(\mathbf{r},\mathbf{r}',\omega) = -\frac{2\omega^2}{\pi}\hat{\mathbf{n}}\cdot\mathbf{G}^{\mathrm{ind}}(\mathbf{r},\mathbf{r}',\omega)\cdot\hat{\mathbf{n}}',$$

which is analytic in the upper part of the complex ω plane and vanishes for large ω in that plane. As a consequence, it satisfies Kramers-Kronig relations, ^{S1} and, in particular,

$$\operatorname{Re}\{f_{\hat{\mathbf{n}},\hat{\mathbf{n}}'}(\mathbf{r},\mathbf{r}',\omega)\} = \frac{2}{\pi} \mathcal{P} \int_0^\infty \frac{\omega' \operatorname{Im}\{f_{\hat{\mathbf{n}},\hat{\mathbf{n}}'}(\mathbf{r},\mathbf{r}',\omega')\}}{\omega'^2 - \omega^2} d\omega',$$

which, for $\omega = 0$, becomes

$$\operatorname{Re}\{f_{\hat{\mathbf{n}},\hat{\mathbf{n}}'}(\mathbf{r},\mathbf{r}',0)\} = \frac{2}{\pi} \mathcal{P} \int_0^\infty \frac{\operatorname{Im}\{f_{\hat{\mathbf{n}},\hat{\mathbf{n}}'}(\mathbf{r},\mathbf{r}',\omega')\}}{\omega'} d\omega'. \tag{1}$$

Taking into account that the $\hat{\mathbf{n}}$ component of the induced field generated by a dipole placed at \mathbf{r}' oscillating at frequency ω along $\hat{\mathbf{n}}'$ is given by S2

$$\hat{\mathbf{n}} \cdot \mathbf{E}^{\text{ind}}(\mathbf{r}, \omega) = -4\pi\omega^2 \hat{\mathbf{n}} \cdot \mathbf{G}^{\text{ind}}(\mathbf{r}, \mathbf{r}', \omega) \cdot \hat{\mathbf{n}}',$$

the left-hand side of Equation (1) reduces to

$$\operatorname{Re}\{f_{\hat{\mathbf{n}},\hat{\mathbf{n}}'}(\mathbf{r},\mathbf{r}',0)\} = \frac{1}{2\pi^2}\hat{\mathbf{n}} \cdot \mathbf{E}^{\operatorname{ind}}(\mathbf{r};\mathbf{r}',\hat{\mathbf{n}}'),$$

where $\mathbf{E}^{\mathrm{ind}}(\mathbf{r}; \mathbf{r}', \hat{\mathbf{n}}')$ is the static field at \mathbf{r} , induced by a unit dipole placed at \mathbf{r}' , oriented along $\hat{\mathbf{n}}'$, due to the presence of the nanostructure. It is important to remark that this field is always a real quantity. Finally, noticing that $\mathrm{Im}\{f_{\hat{\mathbf{n}},\hat{\mathbf{n}}'}(\mathbf{r},\mathbf{r}',\omega)\}/\omega$ is equal to the induced LDOS when $\mathbf{r} = \mathbf{r}'$ and $\hat{\mathbf{n}} = \hat{\mathbf{n}}'$, Equation (1) becomes the LDOS sum rule stated in Equation (2) of the main paper. If, on the other hand, we leave $\mathbf{r} \neq \mathbf{r}'$ and $\hat{\mathbf{n}} \neq \hat{\mathbf{n}}'$, then Equation (1) reproduces the sum rule for the CDOS given in Equation (4) of the main paper.

Method of images for electrostatic problems

In the static limit, i.e., for $\omega=0$, the electric field generated by a dipole placed in the vicinity of a nanostructure can be calculated from the electrostatic potential that solves Poisson's equation. If the structure has enough symmetry, Poisson's equation can be solved analytically using the so-called method of images. S1 This method consists in replacing the nanostructure with a collection of image charges, which generate a potential in the region outside of the nanostructure satisfying the boundary conditions imposed by the geometry of the nanostructure. Thanks to the uniqueness of the solution of Poisson's equation, S1 the potential created by the image charges has to be identical to the potential induced by the nanostructure in its exterior. We use the method of images throughout the paper to calculate the static field appearing on the right-hand side of the sum rule. Although a detailed explanation of this method can be found in most electromagnetism textbooks,

we provide here, for the sake of completeness, a summary of its application to planar and spherical geometries.

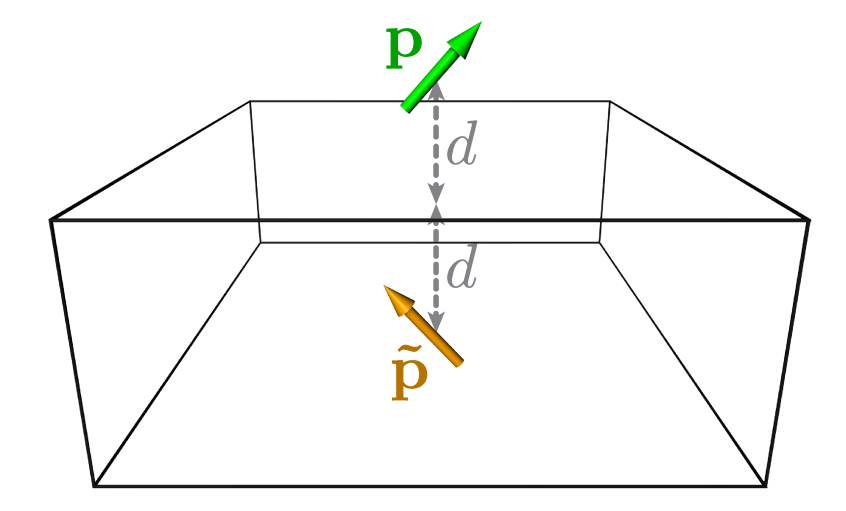


Figure S1: Schematics used in the derivation of the method of images for a dipole placed near an extended planar surface.

Planar surface. We begin by considering the case of a dipole \mathbf{p} , placed at a distance d from a planar surface. The response of the latter caused by the presence of the dipole can be modeled using an image dipole $\tilde{\mathbf{p}}$, placed at the mirror position with respect to the surface, as shown in Figure S1. The electrostatic potential created at \mathbf{r} by a dipole placed at \mathbf{r}' is given by

$$\Phi(\mathbf{r}) = \frac{\mathbf{p} \cdot (\mathbf{r} - \mathbf{r}')}{|\mathbf{r} - \mathbf{r}'|^3},$$

(notice we use Gaussian units) while the corresponding field is

$$\mathbf{E}(\mathbf{r}) = \frac{3(\mathbf{r} - \mathbf{r}')[(\mathbf{r} - \mathbf{r}') \cdot \mathbf{p}]}{|\mathbf{r} - \mathbf{r}'|^5} - \frac{\mathbf{p}}{|\mathbf{r} - \mathbf{r}'|^3}.$$
 (2)

Imposing the continuity of both the tangential component of the electric field and the normal component of the displacement vector, we find that, for a given dipole \mathbf{p} , the corresponding image dipole $\tilde{\mathbf{p}}$ is given by

$$\tilde{\mathbf{p}} = \frac{\varepsilon(0) - 1}{\varepsilon(0) + 1} [2\hat{\mathbf{u}}(\hat{\mathbf{u}} \cdot \mathbf{p}) - \mathbf{p}],$$

where $\hat{\mathbf{u}}$ is the unit vector normal to the surface (pointing outside it), and $\varepsilon(0)$ represents the static value of the dielectric function of the material from which the surface is made. Using these expressions, together with Equation (2), we can calculate the field created by the image dipole at the position of the original dipole, which satisfies

$$\frac{1}{4\pi}\mathbf{E}^{\text{ind}}\cdot\hat{\mathbf{p}}_{\parallel} = \frac{\varepsilon(0)-1}{\varepsilon(0)+1}E_0, \qquad \frac{1}{4\pi}\mathbf{E}^{\text{ind}}\cdot\hat{\mathbf{p}}_{\perp} = \frac{\varepsilon(0)-1}{\varepsilon(0)+1}2E_0,$$

where $\hat{\mathbf{p}}_{\parallel}$ and $\hat{\mathbf{p}}_{\perp}$ are, respectively, unit dipoles parallel and perpendicular to $\hat{\mathbf{u}}$, and $E_0 = 1/(32\pi d^3)$. If the surface is made of a perfect conductor, $\varepsilon(0) \to \infty$, and the expressions above reduce to

$$rac{1}{4\pi}\mathbf{E}^{\mathrm{ind}}\cdot\mathbf{\hat{p}}_{\parallel}=E_{0}, \qquad rac{1}{4\pi}\mathbf{E}^{\mathrm{ind}}\cdot\mathbf{\hat{p}}_{\perp}=2E_{0}.$$

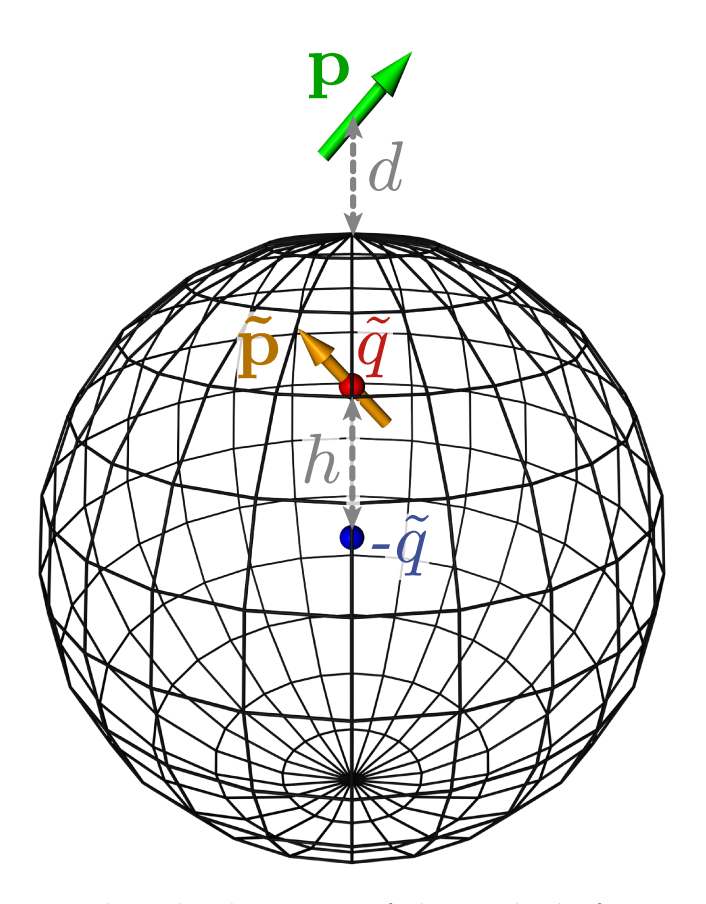


Figure S2: Schematics used in the derivation of the method of images for a dipole placed near a sphere.

If instead, the field of the image dipole is evaluated at a position different from that of the original dipole, we get

$$\frac{1}{4\pi}\mathbf{E}^{\text{ind}} = \frac{3(\mathbf{r} - \mathbf{r}')[(\mathbf{r} - \mathbf{r}') \cdot \tilde{\mathbf{p}}]}{4\pi|\mathbf{r} - \mathbf{r}'|^5} - \frac{\tilde{\mathbf{p}}}{4\pi|\mathbf{r} - \mathbf{r}'|^3},$$

where \mathbf{r} and \mathbf{r}' represent, in this case, the position at which the field is evaluated, and the position at which the image dipole $\tilde{\mathbf{p}}$ is located.

Sphere. The other important geometry we use in the manuscript is that of a dipole placed at a point \mathbf{r} , located at a distance d above the surface of a perfectly conducting sphere of radius R, as shown in Figure S2. Following the derivation by Santos and Tort, ^{S3} we start by considering the case of a grounded sphere, for which the potential must vanish everywhere on its surface. We can model the effect of the sphere by using an image dipole $\tilde{\mathbf{p}}$ and an image charge \tilde{q} , placed at a point $\tilde{\mathbf{r}}$. This point is located on the line connecting the original dipole and the center of the sphere, a distance $h = R^2/(R+d)$ from the latter, as shown in Figure S2. The potential created by the original dipole, the image dipole, and the image charge at a point \mathbf{s} on the surface of the sphere is

$$\Phi(\mathbf{s}) = \frac{\mathbf{p} \cdot (\mathbf{s} - \mathbf{r})}{|\mathbf{s} - \mathbf{r}|^3} + \frac{\tilde{\mathbf{p}} \cdot (\mathbf{s} - \tilde{\mathbf{r}})}{|\mathbf{s} - \tilde{\mathbf{r}}|^3} + \frac{\tilde{q}}{|\mathbf{s} - \tilde{\mathbf{r}}|}.$$

Imposing $\Phi(\mathbf{s}) = 0$, we can solve this equation to obtain

$$\tilde{\mathbf{p}} = \frac{R^3}{(R+d)^3} [2\hat{\mathbf{u}}(\hat{\mathbf{u}} \cdot \mathbf{p}) - \mathbf{p}], \qquad \tilde{q} = \frac{R}{(R+d)^2} (\hat{\mathbf{u}} \cdot \mathbf{p}),$$

where $\hat{\mathbf{u}}$, in this case, is the unit vector normal to the surface of the sphere (pointing outside it) at the point at which it is crossed by the line connecting its center with the position of \mathbf{p} . If instead of having a grounded sphere, we have an isolated sphere, the total image charge has to vanish. We can fulfill this requirement without altering the uniformity of the potential on the surface of the sphere by adding an extra image charge $-\tilde{q}$ at the center of the sphere.

Then, the field created by the image dipole and the two image charges at a point \mathbf{r}' outside the sphere is

$$\mathbf{E}^{\text{ind}}(\mathbf{r}') = \frac{3(\mathbf{r}' - \tilde{\mathbf{r}})[(\mathbf{r}' - \tilde{\mathbf{r}}) \cdot \tilde{\mathbf{p}}]}{|\mathbf{r}' - \tilde{\mathbf{r}}|^5} - \frac{\tilde{\mathbf{p}}}{|\mathbf{r}' - \tilde{\mathbf{r}}|^3} + \tilde{q} \frac{(\mathbf{r}' - \tilde{\mathbf{r}})}{|\mathbf{r}' - \tilde{\mathbf{r}}|^3} - \tilde{q} \frac{\mathbf{r}'}{|\mathbf{r}'|^3}.$$
 (3)

Taking $\mathbf{r}' = \mathbf{r}$, the field at the position of the original dipole due to the presence of the sphere satisfies

$$\frac{1}{4\pi} \mathbf{E}^{\text{ind}} \cdot \hat{\mathbf{p}}_{\parallel} = \frac{8R^3}{(2R+d)^3} E_0, \qquad \frac{1}{4\pi} \mathbf{E}^{\text{ind}} \cdot \hat{\mathbf{p}}_{\perp} = \left[\frac{8R^3}{(2R+d)^3} + \frac{4Rd}{(2R+d)^2} - \frac{4Rd^3}{(R+d)^4} \right] 2E_0,$$

where $\hat{\mathbf{p}}_{\parallel}$ and $\hat{\mathbf{p}}_{\perp}$ are, respectively, unit dipoles parallel and perpendicular to the sphere surface. These expressions, normalized to E_0 , correspond to the solid curves in Figure 1 of the main paper. On the other hand, leaving $\mathbf{r}' \neq \mathbf{r}$, Equation (3) can be used to calculate the right-hand side of the sum rule for the CDOS (solid and dashed curves in Figure 6 of the main paper).

LDOS and CDOS near an extended system

In order to calculate the induced part of the LDOS and the CDOS near an extended system such as a metallic film or graphene sheet, we can take advantage of their translational invariance to write the induced part of the Green tensor connecting points $\mathbf{r} = (x, y, z)$ and $\mathbf{r}' = (x', y', z')$, as S2

$$\mathbf{G}^{\text{ind}}(\mathbf{r}, \mathbf{r}', \omega) = -\frac{i}{8\pi^2 \omega^2} \int_{-\infty}^{\infty} \frac{dQ_x dQ_y}{k_z} e^{iQ_x(x-x')} e^{iQ_y(y-y')} e^{ik_z(z+z')} \left[r_p \mathbf{M}_p + r_s \mathbf{M}_s \right]. \tag{4}$$

where Q_x and Q_y are the components of the wave vector parallel to the surface, while $k_z = \sqrt{k^2 - Q^2}$ is the component perpendicular to it, with $Q^2 = Q_x^2 + Q_y^2$ and $k = \omega/c$. Furthermore, r_p and r_s are the Fresnel reflection coefficients of the extended system for p-

and s-polarized waves, and

$$\mathbf{M}_{p} = \begin{pmatrix} -k_{z}^{2} \frac{Q_{x}^{2}}{Q^{2}} & -k_{z}^{2} \frac{Q_{x}Q_{y}}{Q^{2}} & -Q_{x}k_{z} \\ -k_{z}^{2} \frac{Q_{x}Q_{y}}{Q^{2}} & -k_{z}^{2} \frac{Q_{y}^{2}}{Q^{2}} & -Q_{y}k_{z} \\ Q_{x}k_{z} & Q_{y}k_{z} & Q^{2} \end{pmatrix}, \qquad \mathbf{M}_{s} = \begin{pmatrix} k^{2} \frac{Q_{y}^{2}}{Q^{2}} & -k^{2} \frac{Q_{x}Q_{y}}{Q^{2}} & 0 \\ -k^{2} \frac{Q_{x}Q_{y}}{Q^{2}} & k^{2} \frac{Q_{x}^{2}}{Q^{2}} & 0 \\ 0 & 0 & 0 \end{pmatrix}.$$

Taking the limit $\mathbf{r}' \to \mathbf{r}$, the equation above reduces to

$$\mathbf{G}^{\text{ind}}(\mathbf{r}, \mathbf{r}, \omega) = \frac{i}{8\pi\omega^2} \int_0^\infty dQ \, Q e^{2izk_z} \left[r_p \begin{pmatrix} k_z & 0 & 0 \\ 0 & k_z & 0 \\ 0 & 0 & \frac{-2Q^2}{k_z} \end{pmatrix} - \frac{r_s k^2}{k_z} \begin{pmatrix} 1 & 0 & 0 \\ 0 & 1 & 0 \\ 0 & 0 & 0 \end{pmatrix} \right],$$

from which the induced LDOS can be directly calculated using Equation (1) of the main paper. If, on the other hand, we are interested on the CDOS, we have to work with Equation (4), particularized for the \mathbf{r} and \mathbf{r}' under consideration.

The Fresnel reflection coefficients for the metallic slab of thickness t studied in the paper are given by

$$r_i = \frac{\rho_i (1 - e^{2ik_z't})}{1 - \rho_i^2 e^{2ik_z't}},$$

where i = (p, s), $k'_z = \sqrt{\varepsilon(\omega)k^2 - Q^2}$, $\varepsilon(\omega)$ is the dielectric function of the slab, and ρ_i is the reflection coefficient for a planar interface defined as S2

$$\rho_p = \frac{\varepsilon(\omega)k_z - k_z'}{\varepsilon(\omega)k_z + k_z'}, \qquad \rho_s = \frac{k_z - k_z'}{k_z + k_z'}.$$

Alternatively, for the case of a graphene sheet, we have

$$r_p = \frac{\frac{2\pi\sigma(\omega)}{\omega}k_z}{1 + \frac{2\pi\sigma(\omega)}{\omega}k_z}, \qquad r_s = -\frac{\frac{2\pi\sigma(\omega)\omega}{c^2}}{k_z + \frac{2\pi\sigma(\omega)\omega}{c^2}},$$

where $\sigma(\omega)$ is the graphene conductivity defined in the paper.

Numerical integrations

The sum rule involves an integral over the whole frequency spectrum. In order to calculate it numerically, we must restrict the integral to a finite frequency interval $\omega_{\min} \leq \omega \leq \omega_{\max}$, and then we approximate

$$\int_0^\infty \mathrm{LDOS}_{\hat{\mathbf{n}}}^{\mathrm{ind}}(\omega) d\omega \approx \int_{\omega_{\mathrm{min}}}^{\omega_{\mathrm{max}}} \mathrm{LDOS}_{\hat{\mathbf{n}}}^{\mathrm{ind}}(\omega) d\omega.$$

We choose $\omega_{\rm min}$ and $\omega_{\rm max}$ such that the extension of the frequency interval does not change the result of the integral within our numerical precision. In practice, this results in values of $\omega_{\rm min} \approx 10^{-4}\,{\rm eV}$ and $\omega_{\rm max} \approx 10-50\,{\rm eV}$.

References

- (S1) Jackson, J. D. Classical Electrodynamics; Wiley: New York, 1999.
- (S2) Novotny, L.; Hecht, B. *Principles of Nano-Optics*; Cambridge University Press: New York, 2006.
- (S3) Santos, F. C.; Tort, A. C. The electrostatic field of a point charge and an electrical dipole in the presence of a conducting sphere. *Eur. J. Phys.* **2004**, *25*, 859.